Auto-Calibration Based Control for Independent Metering of Hydraulic Actuators

Patrick Opdenbosch, Nader Sadegh, Wayne Book, Aaron Enes

***Abstract*— This paper describes a novel auto-calibration state-trajectory-based control method and its application to electronic flow control for independent metering systems. In this paper, the independent metering architecture that is considered uses five Electro-Hydraulic Poppet Valves (EHPV's). The proposed control method is applied to four of these valves, arranged in a Wheatstone bridge configuration, to regulate the flow of hydraulic oil coming into and out of an actuator. For simplicity, the fifth valve is operated via open-loop to control the supply pressure. Experimental data presented herein demonstrate that the control method learns the valve's conductance characteristics (i.e. the inverse input-state dynamic map of the valve) while simultaneously controlling the motion of the hydraulic actuator.**

I. Introduction

In recent years, the concept of using Independent Metering Valves (IMV) to control the motion of hydraulic actuators has attracted considerable attention in the fluid power industry. The attention has been focused at using IMV's to improve system efficiency in mechanical manipulators such as hydraulic excavators and backhoes. When compared to traditional systems composed of directional spool valves, IMV's can improve the system's efficiency by switching among metering modes (combinations of flow paths) that allow single/multi-function flow regeneration [4,12,16]. Another advantage of this concept, is the fact that IMV's are solenoid-actuated valves which are controlled electronically [1,2,10]. This allows not only the possibility of enabling automation features for the aforementioned machines, but also the application of intelligent controls. In this paper, a novel auto-calibration state-tracking-based control method is introduced for independent metering valves. The control method simultaneously learns the valve's inverse input-state map (i.e. the conductance characteristics) while using this knowledge to control the valve and in turn control the motion of a given hydraulic actuator.

There are four major advantages of using an auto-calibration based controller for IMV's: *first*, there would be no need to obtain extensive offline calibrations for valves of the same size as it is typically done in industry [10]. With this type of learning/adaptive controller, generic calibration data can be used and the discrepancies are corrected online. *Second*, the IMV's performance can be improved by combining feedback control and active learning-based feedforward compensation. *Third*, an active learning-based auto-calibration scheme can ensure an accurate characterization of the valve is maintained throughout the operational life of the device. *Fourth*, a fault detection scheme can be easily implemented in the control loop by monitoring the valve's deviation from expected performance [7].

The idea of using the inverse mapping of the system for control has been investigated in the past (see for example [6,11,21]). In these works, research has been focused at controlling the outputs of the system rather than the states. In the fluid power industry, controllers with learning capabilities have been attempted in large mechanical manipulators. For example, a coordinated motion controller with learning capabilities was presented by Johnson et al. in [3]. Song and Koivo in [17] used a feedforward multilayered neural network with backpropagation adaptation to model the inverse dynamics of an excavator. Recently, Liu and Yao in [5] proposed the online modeling of the flow mappings for unidirectional cartridge valves using neural networks. In [5], the valve flow mappings were considered as time-invariant and the valve dynamics were neglected.

It should be noted that most of the relevant works found in the literature deal with output tracking error instead of state tracking error. Moreover, for the reasons outlined above, auto-calibration based control schemes have the potential to add value on fluid power components using such strategies. With this in mind, the contribution of this paper is the introduction of an essentially model-free control law that learns the inverse *input-state* dynamic mapping of an IMV while the latter is used in a flow control application.

The rest of the paper is organized as follows: The IMV used herein is introduced first in Section II followed by a description of the experimental testbed (Section III). The overall control architecture is then explained in Section IV while the auto-calibration control scheme is discussed in Section V. Experimental results are given in Section VI followed by the conclusions of the paper.

II. Independent Metering Valve

The Electro-Hydraulic Poppet Valve (EHPV) considered herein is shown in Fig. 1 and amply described in [8,22,23]. This is a valve whose opening is proportional to the amount

This work was completed at the Georgia Institute of Technology and supported by the Fluid Power Motion Control Center and HUSCO Intl.

Patrick Opdenbosch, Ph.D. is a senior research engineer at Caterpillar Inc. Mossville, IL 61552 USA. E-mail: opdenbosch_patrick@cat.com

Nader Sadegh, Ph.D. is an associate professor in the George W. Woodruff School of Mechanical Engineering at the Georgia Institute of Technology, Atlanta GA, 30332, USA. E-mail: nader.sadegh@me.gatech.edu

Wayne Book, Ph.D., is the HUSCO/Ramirez Distinguished professor in Fluid Power and Motion Control in the George W. Woodruff School of Mechanical Engineering at the Georgia Institute of Technology, Atlanta GA, 30332, USA. E-mail: wayne.book@me.gatech.edu

Aaron Enes, Ph.D. is a member of the technical staff at MIT Lincoln Laboratory, Lexington MA, 02420, USA. E-mail: Aaron.Enes@ll.mit.edu

of current sent to its solenoid (a nonlinear relationship). In addition, this valve has two main distinguishing features: *first* this valve possesses an internal pressure compensation mechanism. This mechanism ensures that the minimum amount of solenoid current needed to crack the valve open is always consistent [18,23]. *Second*, this valve is bidirectional, a feature that is essential to accomplish regenerative flow operations of hydraulic actuators [20]. Other features include virtually 'zero' leakage (1.25 cm^3/min at 10 MPa) and low hysteresis (less than 5%).

In this paper, each EHPV is controlled by changing its *conductance* parameter, denoted by Kv. The valve's conductance, a measure of the valve's opening, is computed using $Kv = |Q|/\sqrt{|\Delta P|}$ (whenever $\Delta P \neq 0$), where Q is the flow through the valve and ΔP is the pressure difference across the same. The valve's conductance is controlled by sending current to the valve's solenoid via Pulse-Width-Modulation (PWM). For a given solenoid current, the EHPV's employed herein are capable of maintaining a constant Kv independent of the pressure difference across the valve if the latter is higher than 0.4 MPa [9]. Although EHPV's are highly nonlinear with complex dynamics, experiments have shown that these EHPV's can be considered as first order (single state) nonlinear systems whose input is the solenoid current i_{sol} and whose single state and output are the valve's conductance Kv [8].

III. Hydraulic Testbed

The motion control of a hydraulic actuator using IMV's is accomplished herein using five (5) EHPV's as shown in Fig. 2. The EHPV labeled 'Valve SR' is used to control the supply pressure P_S. The other four EHPV's are part of a Wheatstone bridge arrangement and accomplish a powered extension or powered retraction of the actuator by controlling hydraulic flow. The hydraulic piston actuates a rotating linkage that raises or lowers a 445 N load. Furthermore, the pressures labeled P_S, P_A, P_B,and P_R as well as the piston's position

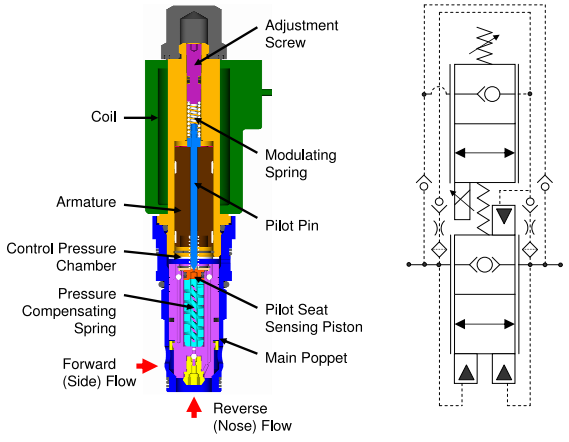

Fig. 1. Components of the Electro-Hydraulic Poppet Valve (left) and its detailed hydraulic symbol (right)

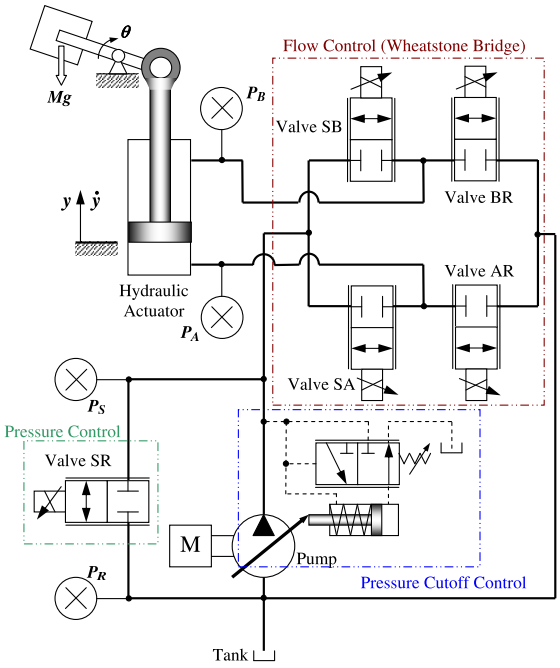

Fig. 2. Schematic of the hydraulic testbed (EHPV's are depicted as two-way two-position valves for simplicity)

y and velocity $\dot{y}$ are available via CAN bus communication for feedback.

The testbed uses a Vickers PVB20 pressure compensated variable displacement piston pump. The pump is driven by a 25 hp Delco electrical motor whose speed is kept constant at 1755 rpm. The maximum displacement of the pump is 42.8 mL/rev, and as shown in [9], it has a pressure cutoff setting of 8 MPa.

IV. Control Architecture

The complete control architecture is shown in Fig. 3. An operator commands the system by moving a joystick into a desired position. The position of the joystick r gets converted into a normalized velocity command $\eta \in [-1, 1]$ in the 'operator interface' module[1]. This module also receives the inferred maximum attainable velocity $\dot{y}_{\max}$ from the 'flow management' module. The 'flow management' module receives the supply pressure P_S and passes it through a lookup table to compute the available flow from the pump $Q_p = \Gamma(P_S)$ [9]. The parameter $\dot{y}_{\max}$ is then calculated by $\dot{y}_{\max} = Q_p/A^*(\eta)$ using

$$A^*(\cdot) = A_B + \frac{A_A - A_B}{2}(sgn(\cdot) + 1) \qquad (1)$$

where $A_A = 5442$ mm^2 is the cap-side area of the piston, $A_B = 3889$ mm^2 is the rod-side area of the piston, and $sgn(\cdot)$ represents the sign function. The output of the 'operator interface' module is the commanded piston velocity $\dot{y}_{\text{cmd}} = \eta \dot{y}_{\max}$, which is then passed to the 'INCOVA logic'

[1]By convention, positive commands are associated to piston extension while negative commands are associated to piston retraction.

module, discussed in Section IV-A, and the 'pump control' module.

The 'pump control' module has the task of controlling the supply pressure P_S. It receives the workport pressures P_A and P_B and computes the commanded conductance $Kv_{\text{SR}}^{\text{cmd}}$ for the 'SR' valve using

$$Kv_{\text{SR}}^{\text{cmd}} = \frac{\Gamma\left(P_S^*\right) - \dot{y}_{\text{cmd}} A^*\left(\dot{y}_{\text{cmd}}\right)}{\sqrt{P_S^* - P_R}} \tag{2}$$

$$P_S^* = \begin{cases} \max\left(P_A + \Delta_p, P_A^{\min}\right) & \text{if } \dot{y}_{\text{cmd}} \geq 0 \\ \max\left(P_B + \Delta_p, P_B^{\min}\right) & \text{else} \end{cases} \tag{3}$$

For this particular testbed, the pump margin was set to $\Delta_p = 2.0$ MPa and the minimum pressures were set to $P_A^{\min} = P_B^{\min} = 2.5$ MPa. The computed $Kv_{\text{SR}}^{\text{cmd}}$ parameter is then passed through the corresponding 'inverse calibration' module. As it can be seen in Fig. 3, there is an 'inverse calibration' module for each EHPV. These modules are used to compute the solenoid current command for the corresponding valve (e.g. $i_{\text{SR}}^{\text{cmd}} = \Lambda\left(Kv_{\text{SR}}^{\text{cmd}}\right)$). Each calibration map $\Lambda : \mathbb{R} \to \mathbb{R}$ is obtained from the steady state current vs. conductance characteristics for the corresponding valve. Likewise, there is a 'PWM driver' for each valve. These drivers receive the corresponding solenoid current command in mA and use an internal analog feedback controller to deliver the current to the appropriate solenoid via Pulse-Width-Modulation. Lastly, the 'Kv measurement' module receives the measured piston's velocity $\dot{y}$ along with the system pressures and computes the actual Kv for each valve. The 'Kv measurement' module is only activated when the auto-calibration controller, explained in Section V, is used. The entire control architecture is implemented using MATLAB's XPC target tool and run at a sampling period of 10 ms (i.e. sampling at a frequency of 100 Hz).

A. INCOVA Logic Module

The 'INCOVA logic' module, invented by Pfaff and Tabor [10], receives the commanded velocity $\dot{y}_{\text{cmd}}$ along with the system's pressures and in turn computes the conductance coefficient for each valve in the Wheatstone bridge. This is accomplished by first computing the parameter Kv_{EQ} using (4) according to [10,19,20] (see appendix for the derivation).

$$Kv_{EQ} = \frac{|P_{EQ}|}{P_{EQ}} \frac{\dot{y}_{\text{cmd}} A_B}{\sqrt{|P_{EQ}|}} \tag{4}$$

The computation of Kv_{EQ} requires knowledge of the pressure parameter P_{EQ} given by

$$P_{EQ} = R\left(P_1 - P_A\right) + \left(P_B - P_2\right) \tag{5}$$

where $R = A_A/A_B$, and the working pressures P_1 and P_2 are obtained from Table I depending on the appropriate metering mode.

The parameter Kv_{EQ} is related to the active valves via (6). The active valves, which use the subscripts α and β, are given in Table I for the appropriate metering mode.

$$Kv_{EQ} = \frac{Kv_\alpha Kv_\beta}{\sqrt{Kv_\beta^2 R^3 + Kv_\alpha^2}} \tag{6}$$

Once the parameter Kv_{EQ} is known, all four valve conductances are computed according to [10,19,20] as

$$Kv_\alpha = \sqrt{\mu^2 + R^3} Kv_{EQ} \tag{7}$$

$$Kv_\beta = \mu^{-1} Kv_\alpha \tag{8}$$

$$Kv_\gamma = Kv_\delta = 0 \tag{9}$$

where μ is the conductance or opening ratio. If this parameter is set to $\mu = R$, then the valves are opened aiming at having equal pressure drops. In this case, the opening ratio is set to $\mu = R^{3/4}$ to minimize the impact errors in valve conductance have on achieving the commanded piston's velocity $\dot{y}_{\text{cmd}}$ [10, 19,20].

Next, constraints are introduced for the computed conductances of the active valves to prevent cavitation (minimum workport pressure $P_i^{\min}$), overpressurization (maximum workport pressure $P_i^{\max}$), and to avoid exceeding valve opening capabilities. As such,

$$Kv_\alpha^{\text{cmd}} = \max\left\{\min\left\{Kv_\alpha, Kv_\alpha^{\max}\right\}, Kv_\alpha^{\min}\right\} \tag{10}$$

$$Kv_\beta^{\text{cmd}} = \max\left\{\min\left\{Kv_\beta, Kv_\beta^{\max}\right\}, Kv_\beta^{\min}\right\} \tag{11}$$

where the limits are obtained from (Θ denotes min or max)

$$Kv_\alpha^\Theta = \Theta\left\{\Psi_1^A(\min), \Psi_1^A(\max), 0, \bar{K}v_\alpha\right\} \tag{12}$$

$$Kv_\beta^\Theta = \Theta\left\{\Psi_2^B(\min), \Psi_2^B(\max), 0, \bar{K}v_\beta\right\} \tag{13}$$

$$\Psi_i^w(h) = \frac{A_w \dot{y}_{\text{cmd}} sgn\left(P_i - P_w^h\right)}{\sqrt{|P_i - P_w^h|}} \tag{14}$$

In these constraints, $\bar{K}v_\alpha$ and $\bar{K}v_\beta$ represent the maximum valve coefficients that are physically attainable for Kv_α and Kv_β respectively. The constraints are applied to satisfy the following priorities:

1) Constrain valve conductance to physically realizable limits
2) Satisfy pressure constraints $P_i^{\min}$ and $P_i^{\max}$
3) Achieve desired piston velocity $\dot{y}_{\text{cmd}}$
4) Use $\mu = R^{3/4}$ to minimize $e_v = \dot{y} - \dot{y}_{\text{cmd}}$

V. Auto-Calibration Controller

The overall control architecture presented so far employs 'inverse calibration' modules that contain non-adaptive lookup tables $\Lambda(\cdot)$. In what follows, each 'inverse calibration' module shown in Fig. 3, except the one used for valve 'SR', will be enhanced with an auto-calibration controller. For this purpose, the 'Kv measurement' module is enabled. At every sampling instant, this module feeds back the active valves' measured conductances using the equation $Kv_{ij} = |\dot{y}|\, A^*(\dot{y}) / \sqrt{|P_i - P_j|}$.

TABLE I
METERING MODES AND CORRESPONDING PARAMETERS USED FOR K_{EQ} AND P_{EQ}

Metering Mode	P_1	P_2	α	β	γ	δ
Powered Extension ($\dot{y} \geq 0$)	P_S	P_R	SA	BR	SB	AR
Powered Retraction ($\dot{y} < 0$)	P_R	P_S	AR	SB	SA	BR

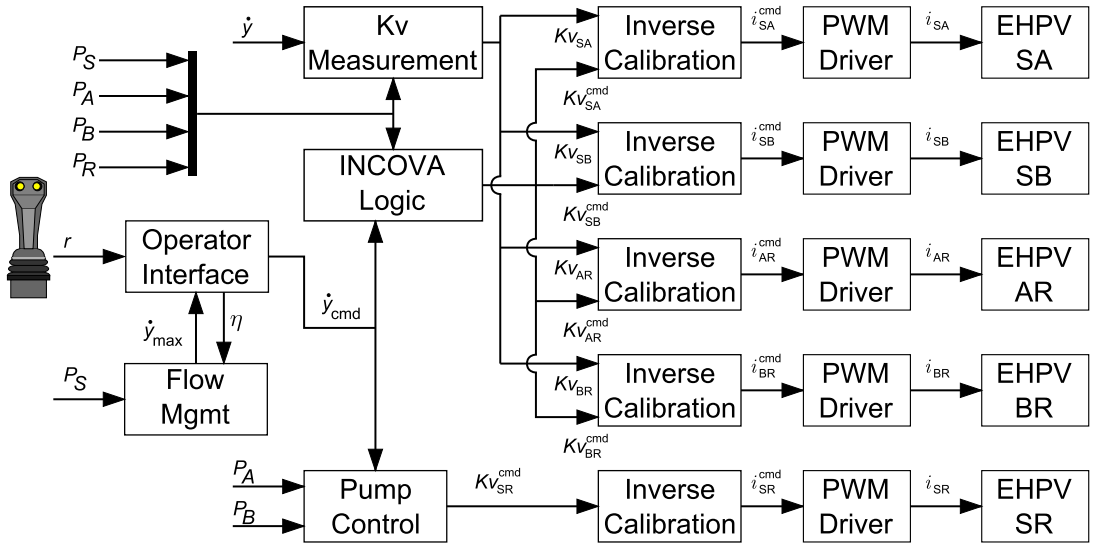

Fig. 3. Schematic of the overall control architecture

The auto-calibration control law presented hereafter is equally applied to each valve in the Wheatstone bridge. This controller uses a Nodal-Link-Perceptron-Network (NLPN) in the feedforward loop. This is a perceptron-type neural network architecture developed by Sadegh in [13,14,15] that can be understood as an adaptive look-up table. At every sampling instant, the NLPN receives the commanded conductance Kv^{cmd} and computes the corresponding solenoid current[2] i_{sol} according to

$$i_{\text{sol}} = \hat{\mathbf{W}}^T \Phi\left(x_1, x_2\right) + \Lambda\left(x_1\right) \tag{15}$$

where $x_1 = Kv^{\text{cmd}}$, and $x_2 = \Delta Kv^{\text{cmd}}$. The latter parameter, included to distinguish steady state and dynamic valve response, represents the time derivative of Kv^{cmd} and is computed by taking the difference between the current and past sampled values of Kv^{cmd}. Moreover, in (15), $\hat{\mathbf{W}} \in \mathbb{R}^N$ is the vector of adjustable weights applied to the basis function vector $\Phi = \left[\phi_{1,1}\left(x_1, x_2\right), \ldots, \phi_{n_1,n_2}\left(x_1, x_2\right)\right]^T$. The basis function vector contains a total of N piecewise linear activation functions $\phi : \mathbb{R}^2 \rightarrow \mathbb{R}$ where $N = n_1 \times n_2$ represents the number of nodal points chosen by the user. The output of $\phi_{i,j}\left(x_1, x_2\right)$ is computed from

$$\phi_{i,j}\left(x_1, x_2\right) = \varphi_{i,1}\left(x_1\right) \varphi_{j,2}\left(x_2\right) \tag{16}$$

$$\varphi_{m,z}\left(x_z\right) = \begin{cases} \frac{\left(x_z - \lambda_{m-1,z}\right)}{\left(\lambda_{m,z} - \lambda_{m-1,z}\right)} & \text{if } x_z \in \left[\lambda_{m-1,z}, \lambda_{m,z}\right) \\ \frac{\left(x_z - \lambda_{m+1,z}\right)}{\left(\lambda_{m,z} - \lambda_{m+1,z}\right)} & \text{if } x_z \in \left[\lambda_{m,z}, \lambda_{m+1,z}\right] \\ 0 & \text{else} \end{cases} \tag{17}$$

for $i \times j = \{1, \ldots, n_1\} \times \{1, \ldots, n_2\}$. The values $n_1 - 1$ and $n_2 - 1$ represent the number of divisions the user selects for the x_1-axis and x_2-axis respectively to form the NLPN input space grid. The grid points establishing these divisions are denoted by $\lambda_{\cdot,1}$ and $\lambda_{\cdot,2}$ for the x_1-axis and x_2-axis respectively. In addition, $\lambda_{0,1}$, $\lambda_{0,2}$, $\lambda_{n_1+1,1}$, and $\lambda_{n_2+1,2}$ are artificially set to ∞.

At the same time the NLPN is used for feedforward control, it is simultaneously trained via the following steepest descent adaptation

$$\hat{\mathbf{W}}^+ = \hat{\mathbf{W}} + \gamma \Phi\left(x_1, x_2\right) e \tag{18}$$

where $e = Kv^{\text{cmd}} - Kv$ is the state trajectory error for the EHPV. The superscript '+' is used to denote the next sampling instance of the parameter $\hat{\mathbf{W}}$ given its present sampled value $\hat{\mathbf{W}}$ and the present sampled values for x_1, x_2, and e. Note that the term $\Lambda\left(\cdot\right)$ can be dropped from (15) if the vector of adjustable weights $\hat{\mathbf{W}}$ is initialized with available steady state data. Also, it is important to mention that the learning rate γ must be chosen such that $0 \leq \gamma \left|\Phi\left(x_1, x_2\right)\right|^2 < 2$ to ensure closed loop stability (see [7,14]). Moreover, in this case, the learning rate γ is set to 0 if the desired state trajectory Kv^{cmd} is not a persistently exciting signal (see [7]).

VI. Experimental Results

The response of the system subject to this control system, with and without adaptation in the 'inverse calibration' modules, is given in the following figures. Note that for the case presented in these figures, the commanded velocity was generated by the XPC-target computer as a periodic and smooth signal for comparison purposes. Fig. 4 shows the commanded piston velocity 'Vcmd' along with the measured piston velocity without adaptation 'Vm NL' and with adaptation 'Vm L'. Likewise, all the system pressures are included in this figure. Fig. 5 shows the individual commanded conductances along with the measured individual conductances with and without adaptation. For example, 'KSAc L' is the commanded conductance for valve 'SA', and 'KSAm

[2]For example, $i_{\text{sol}} = i_{\text{SA}}^{\text{cmd}}$ if $Kv^{\text{cmd}} = Kv_{\text{SA}}^{\text{cmd}}$.

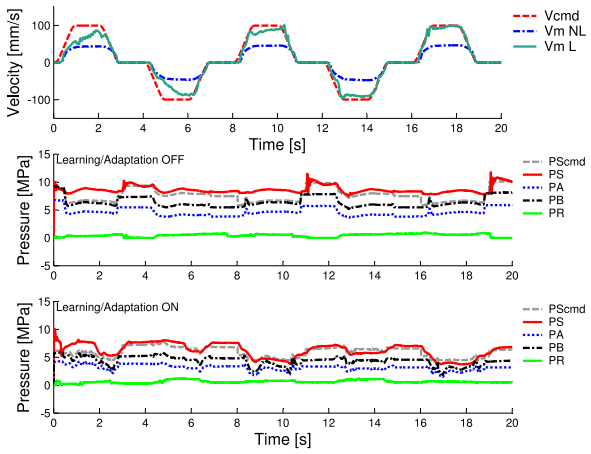

Fig. 4. Overall system response with and without learning/adaptation

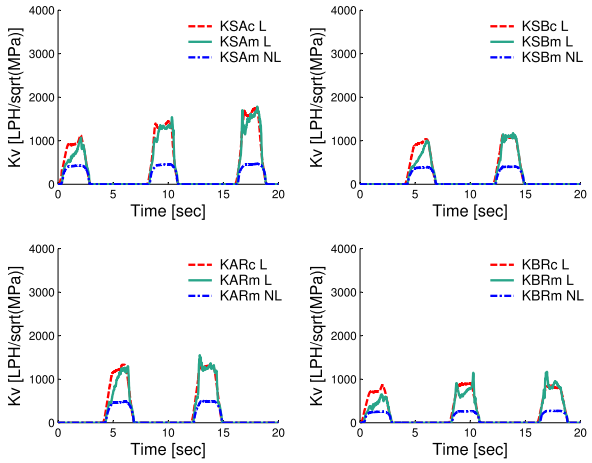

Fig. 5. Flow conductance performance with and without adaptation for the EHPV's in the Wheatstone bridge

L' is the measured conductance when learning/adaptation is enabled. Furthermore, 'KSAm NL' is the measured conductance when learning/adaptation is disabled. As evidenced in these figures, good tracking performance is achieved with the learning/adaptive controller in a few cycles. Because of limitations arising from the linkage's range of motion and the pump capabilities, higher piston speeds and thus higher conductance values were not attempted.

When the learning/adaptation was enabled, the NLPN weights were initialized to zero and (18) was used to update the weights with a learning rate γ of[3] 0.015. Moreover, the NLPN's input space was partitioned with the grid vectors,

$$x_{1\_\text{grid}} = [\lambda_{1,1}, \ldots, \lambda_{9,1}] = [0, 1, 100, 600, 800, 1000, 2000, 5000, 10000] \quad (19)$$

$$x_{2\_\text{grid}} = [\lambda_{1,2}, \ldots, \lambda_{5,2}] = [-40000, -0.01, 0, 0.01, 40000] \quad (20)$$

Consequently, the number of nodal points for the NLPN (i.e. the NLPN's size) was $N = 9 \times 5 = 45$. The size of the NLPN can be increased to improve accuracy in the learned inverse input-state map at the expense of increasing computational burden.

The steady state characteristics of valve 'SR' were measured in a separate valve body and used to create the generic inverse input-state calibration $\Lambda(\cdot)$. For illustration purposes, this calibration was scaled down by 10% and used in all 'inverse calibration' modules. The generic calibration is shown along with the learned calibrations in Fig. 6. Note that vertical lines were added in these plots to help the reader visualize the grid vector x_{1_grid}. Additionally, notice that the learned calibrations differ from the generic one mostly around[4] 800-2000 LPH/sqrt(MPa), which is the region of the NLPN's input space where most of the experiment took place (see Fig. 5). It is in this region that the control system corrected the generic calibration map.

[3]Increasing the learning rate has the trade off that performance during learning/adaptation may be less smooth.

[4]1 LPH = 1 L/hr = $2.8 \times 10^{-7} \text{m}^3/\text{s}$

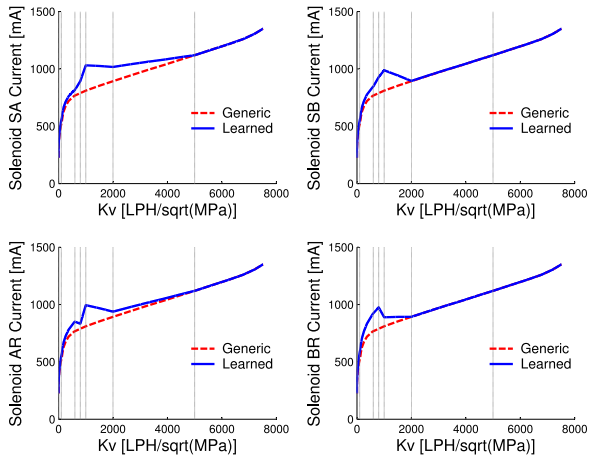

Fig. 6. Generic and learned calibration characteristics for the EHPV's in the Wheatstone bridge

VII. Conclusions

This paper presented the application of an auto-calibration based control method for EHPV's. More specifically, the use of this controller for independent metering of a hydraulic actuator during a powered extension and a powered retraction were considered in this case. Other metering modes were not explored and will be left for future research. The control law presented herein simultaneously corrected a generic inverse input-state mapping of the EHPV while forcing its conductance coefficient to follow a prescribed desired trajectory. Experimental results showed that it was possible to achieve good tracking of the commanded piston's velocity by using the proposed controller in conjunction with open-loop control of the supply pressure. It was also shown that this was possible while using a relatively small number of nodal points for the NLPN.

VIII. Acknowledgments

The authors thank the support provided to this project by HUSCO International and the Fluid Power Motion Control

Center at Georgia Tech.

IX. Appendix

The derivation of the Kv_{EQ} and P_{EQ} parameters is presented next under the following assumptions:

1) Quasi-static hydraulic piston motion
2) Fluid is incompressible
3) Fluid inertance is negligible
4) Fluid temperature is constant
5) Negligible cylinder crossport leakage

Using Assumption 1 and summing forces on the hydraulic piston yields the following algebraic relationship between workport pressures P_A and P_B, load F_{load}, and friction forces $f(\dot{y})$

$$P_A A_A - P_B A_B = F_{load} + f(\dot{y}) := F_h \tag{21}$$

With the aid of Assumption 3, it is not difficult to realize that

$$Q_\alpha = \operatorname{sgn}(P_1 - P_A) K v_\alpha \sqrt{|P_1 - P_A|} \tag{22}$$

$$Q_\beta = \operatorname{sgn}(P_B - P_2) K v_\beta \sqrt{|P_B - P_2|} \tag{23}$$

where the subscripts α and β represent the active valves according to Table I. Likewise, from conservation of mass and using Assumptions 2 through 5, one finds that the metering flows are related to the piston's velocity by $Q_\alpha = \dot{y} A_A$ and $Q_\beta = \dot{y} A_B$. Hence, $Q_\alpha = R Q_\beta$ where R is the area ratio. Substituting these relationships into (22) and (23) and using the form $Q|Q| = Kv^2 \Delta P$ yields

$$P_A = P_1 - \dot{y}|\dot{y}| \left(\frac{R A_B}{K v_\alpha} \right)^2 \tag{24}$$

$$P_B = \dot{y}|\dot{y}| \left(\frac{A_B}{K v_\beta} \right)^2 + P_2 \tag{25}$$

Substitution of these results into 21 yields

$$\frac{F_h}{A_B} = R \left(P_1 - \dot{y}|\dot{y}| \frac{(R A_B)^2}{K v_\alpha^2} \right) - \dot{y}|\dot{y}| \frac{A_B^2}{K v_\beta^2} - P_2 \tag{26}$$

Upon algebraic manipulation and the use of 21 to substitute for F_h, one finds that

$$\left(\frac{K v_\beta^2 R^3 + K v_\alpha^2}{K v_\alpha^2 K v_\beta^2} \right) \dot{y}|\dot{y}| A_B^2 = R(P_1 - P_A) + (P_B - P_2) \tag{27}$$

which can be rewritten as $\dot{y}|\dot{y}| A_B^2 = K v_{EQ}^2 P_{EQ}$ where Kv_{EQ} is given by (6) and P_{EQ} is given by (5).

References

[1] J. A. Aardema and D. W. Koehler, "System and method for controlling an independent metering valve," U.S. Patent 5,947,140, September, 1999.

[2] A. Jansson and J. Palmberg, "Separate controls of meter-in and meter-out orifices in mobile hydraulic systems," *SAE Transactionsn*, vol. 99, no. 2, pp. 377–383, 1990.

[3] D. W. Johnson, I. Lovell, G. H., and J. J. Murray, "Development of a coordinated motion controller for a front shovel excavator," in *ANS 7th Topical Meeting on Robotics and Remote Systems*, vol. 1, 1997, pp. 239–46.

[4] S. Liu and B. Yao, "Coordinate control of energy-saving programmable valves," in *ASME The Fluid Power and Systems Technology Division*, vol. 10, 2003, pp. 123–131.

[5] ——, "On-board system identification of systems with unknown input nonlinearity and system parameters," *ASME Dynamic Systems and Control Division*, vol. 74, pp. 1079–1085, 2005.

[6] A. Malinowski, J. M. Zurada, and J. H. Lilly, "Inverse control of nonlinear systems using neural network observer and inverse mapping approach," in *IEEE International Conference on Neural Networks - Conference Proceedings*, vol. 5, 1995, pp. 2513–2518.

[7] P. Opdenbosch, "Auto-calibration and control applied to electro-hydraulic valves," Ph.D. Dissertation, Georgia Institute of Technology, 2007.

[8] P. Opdenbosch, N. Sadegh, W. J. Book, T. Murray, and R. Yang, "Modelling an electro-hydraulic poppet valve," *International Journal of Fluid Power*, vol. 10, no. 1, pp. 7–16, 2009.

[9] P. Opdenbosch, N. Sadegh, and W. J. Book, "Learning control applied to electro-hydraulic poppet valves," in *American Control Conference*, 2008, pp. 1525–1532.

[10] J. L. Pfaff and K. A. Tabor, "Velocity based electronic control system for operating hydraulic equipment," U.S. Patent 6,732,512, May, 2004.

[11] D. T. Pham and S. J. Oh, "Adaptive control of dynamic systems using neural networks," in *International Conference on Systems, Man and Cybernetics. Systems Engineering in the Service of Humans*, vol. 4, 1993, pp. 97–102.

[12] B. J. Roberts, "Poppet valves for directional control," *Machine Design*, vol. 60, pp. 119–22, 1988.

[13] N. Sadegh, "A multilayer nodal link perceptron network with least squares training algorithm," *International Journal of Control*, vol. 70, no. 3, pp. 385–404, 1998.

[14] ——, "Nonlinear identification and control via neural networks," in *Winter Annual Meeting of the American Society of Mechanical Engineers*, vol. 33, 1991, pp. 46–56.

[15] ——, "A nodal link perceptron network with applications to control of a nonholonomic system," *IEEE Transactions on Neural Networks*, vol. 6, no. 6, pp. 1516–1523, 1995.

[16] A. Shenouda, "Quasi-static hydraulic control systems and energy savings potential using independent metering four-valve assembly configuration," Ph.D. Dissertation, Georgia Institute of Technology, 2006.

[17] B. Song and A. J. Koivo, "Neural adaptive control of excavators," in *IEEE/RSJ International Conference on Intelligent Robots and Systems*, vol. 1, 1995, pp. 162–7.

[18] D. B. Stephenson, "Auto-calibration of a solenoid operated valve," U.S. Patent 6,397,655, June, 2002.

[19] K. A. Tabor, "Velocity based method for controlling a hydraulic system," U.S. Patent 6,718,759, April, 2004.

[20] ——, "A novel method of controlling a hydraulic actuator with four valve independent metering using load feedback," in *SAE Commercial Vehicle Engineering Congress and Exhibition*, 2005.

[21] B. Widrow, D. Shur, and S. Shaffer, "On adaptive inverse control," in *15th Asilomar Conference on Circuits, Systems and Computers*, 1982, pp. 185–9.

[22] X. Yang, "Pilot solenoid control valve with pressure responsive diaphragm," U.S. Patent 6,149,124, November, 2000.

[23] X. Yang, J. L. Pfaff, and M. J. Paik, "Pilot operated control valve having a poppet with integral pressure compensating mechanism," U.S. Patent 6,745,992, June, 2004.